



**HAL**  
open science

## Electrochemiluminescence Imaging for Bioanalysis

Jingjing Zhang, Stéphane Arbault, Neso Sojic, Dechen Jiang

► **To cite this version:**

Jingjing Zhang, Stéphane Arbault, Neso Sojic, Dechen Jiang. Electrochemiluminescence Imaging for Bioanalysis. *Annual Review of Analytical Chemistry*, 2019, 12 (1), pp.275-295. 10.1146/annurev-anchem-061318-115226 . hal-02374932

**HAL Id: hal-02374932**

**<https://hal.science/hal-02374932>**

Submitted on 17 Dec 2020

**HAL** is a multi-disciplinary open access archive for the deposit and dissemination of scientific research documents, whether they are published or not. The documents may come from teaching and research institutions in France or abroad, or from public or private research centers.

L'archive ouverte pluridisciplinaire **HAL**, est destinée au dépôt et à la diffusion de documents scientifiques de niveau recherche, publiés ou non, émanant des établissements d'enseignement et de recherche français ou étrangers, des laboratoires publics ou privés.

## Electrochemiluminescence Imaging for Bioanalysis

Jingjing Zhang<sup>1</sup>, Stéphane Arbault<sup>2</sup>, Neso Sojic<sup>2\*</sup>, Dechen Jiang<sup>1\*</sup>

<sup>1</sup> State Key Laboratory of Analytical Chemistry for Life Science, School of Chemistry and Chemical Engineering, Nanjing University, Nanjing, Jiangsu 210093, China;

<sup>2</sup> University of Bordeaux, Bordeaux INP, ISM, UMR CNRS 5255, 33607 Pessac, France.

Corresponding Authors: Neso Sojic and Dechen Jiang

Email: [dechenjiang@nju.edu.cn](mailto:dechenjiang@nju.edu.cn) (D. J); [neso.sojic@enscbp.fr](mailto:neso.sojic@enscbp.fr) (N. S)

Email of the other two authors:

Jingjing Zhang <[623771118@qq.com](mailto:623771118@qq.com)>

stephane.arbault <[stephane.arbault@u-bordeaux.fr](mailto:stephane.arbault@u-bordeaux.fr)>

**Abstract.** Electrochemiluminescence (ECL) is a widely used analytical technique with the advantages of high sensitivity and low background signal. The recently fast development of electrochemical materials, luminophores and optical elements significantly increase the ECL signals, and thus, the ECL imaging with enhanced spatial and temporal resolutions is realized. Currently, ECL imaging has been successfully applied in high throughput bioanalysis and to visualize the distribution of molecules at single cells. Compared with other optical bioassays, no optical excitation is involved in imaging approach so that it avoids background signal from the illumination and increases the detection sensitivity. This review highlights some of the most exciting developments in this field, including the mechanisms, the electrode designs and the applications of ECL imaging in bioanalysis and at single cells and particles.

**Keywords.** Electrochemiluminescence imaging, spatial/temporal resolutions, multiplex bioassay, single cells/particles, co-reactant pathway, bipolar electrochemistry

## 1. Introduction.

Electrochemiluminescence or electrogenerated chemiluminescence (ECL) is a versatile and powerful analytical technique widely used in different fields, ranging from fundamental research to commercial clinical and biological applications.<sup>1,2</sup> The initial discovery of ECL emission was reported by Hercules and Bard et al. in the mid-1960s.<sup>3,4</sup> Principally, ECL is a luminescence process resulting from the relaxation of electronically excited products to the ground state after an electrochemical reaction overall combining an electrochemical initiation step and an optical readout.<sup>5</sup> ECL offers remarkable advantages by comparison to other transduction methods: high sensitivity, extremely wide dynamic range, very low background signal, good temporal and spatial control, and insensitivity to matrix effects. Moreover, since this process utilizes the chemical conversion of the analyte at an electrode surface generating the signal, it does not require a recognition probe to bind the target minimizing cellular machinery perturbations.<sup>6</sup> Accordingly, numerous ECL based assay formats, biosensors or analytical strategies have been reported, as reviewed in reference 1,2,7 and 8.

Considering the optical readout in ECL, an important development of this technique is its implementation to visualize the electrochemical process at electrode surfaces. Compared with other optical bioassays, ECL obviously does not require any optical excitation so that it avoids background from scattered light or sample auto-fluorescence. The pioneer works on ECL imaging were conducted by Engstrom et al. to visualize the electrode heterogeneity and to characterize electrode kinetics at microscopic scale.<sup>9-12</sup> The following ECL imaging at arrays of microelectrode exhibited both high sensitivity and high resolution to profile the species over the electrode surface.<sup>13-16</sup> These important breakthroughs result in an emerging electrochemical imaging approach for parallel measurement of samples, or observation of electrochemical and/or biological events at the regions of interest (ROI), such as uneven cellular effluxes associated with heterogeneous distribution of exocytotic microdomains in cells. Different from the classic scanning electrochemical microscopy using a micro/nano-electrode to scan the object<sup>17-20</sup>, the parallel recording of luminescence generated from the surface permit the acquisition of spatially and temporally resolved electrochemical signals.

Despite many advances of ECL imaging, the development of this approach is relative slow as compared with the fluorescence imaging. In the fluorescence process, the atoms in the dye absorb the photon and reach the excited singlet state leading to the emission of a photon with lower energy. However, ECL describes the process where photons are emitted without photo-excitation. Therefore, the main obstacle for ECL imaging is the limited amount of photons (luminescence) produced from the luminescent probe in sub-micron sized ROIs, which is hardly collected even by a single photon counter. The addition of concentrated co-reactant or more alkali into the reaction enhance ECL significantly, however, the use of biologically incompatible solvents restricts the application of ECL imaging for the bioanalysis.

In the past ten years, thanks to the improvement of single photon counter devices, microscopy objectives with greater numerical aperture (N.A.) and optimized light transduction pathways, the detection efficiency of weak luminescence was greatly improved. Moreover, the appearance of new materials with excellent electrochemical properties accelerates the reaction rate of luminophore emitting higher luminescence. Coupled with novel electrode designs and detection strategies, the spatial and temporal resolutions in ECL imaging reach nanometer level and millisecond level, respectively. As a result, high throughput and/or local study in bioanalysis using ECL imaging is realized. In this review, the mechanisms, the electrode designs and the bioanalytical applications, including at single cells and particles, are summarized and discussed.

## 2. Mechanisms and Apparatus of ECL imaging

### 2.1 Co-reactant pathway in ECL imaging

ECL processes can be divided into two main dominant mechanisms: the annihilation pathway and the co-reactant pathway. The earliest ECL reactions were reported by the annihilation mode where an oxidized and a reduced species are electrochemically produced at an electrode surface by applying alternating pulsed potentials<sup>21-23</sup>. Then, these two radicals react together in the diffusion layer according to an annihilation reaction to generate the excited state of the luminophore. Finally, it relaxes to the ground state and emits a photon.

However, a major limitation for bioanalytical applications is that this pathway is limited to aprotic solvents. An alternative mode of ECL generation with more complex mechanisms is based on the use of co-reactants. In the early 1980s, the discovery of ECL in aqueous phase involving  $[\text{Ru}(\text{bpy})_3]^{2+}$  as a luminophore and a sacrificial co-reactant opened a new area<sup>24-26</sup>. The large majority of ECL imaging in bioanalysis is based on a mechanism involving the reaction of a co-reactant species with the luminophore by applying a single anodic potential. One of the most widely used ECL imaging systems is currently the organometallic  $[\text{Ru}(\text{bpy})_3]^{2+}$  complex with amine-based co-reactants, such as tripropylamine (TPrA) or 2-(dibutylamino) ethanol. Since  $[\text{Ru}(\text{bpy})_3]^{2+}$  species could be linked to proteins, this ECL imaging system is mainly applied for immunoassays. Another classic ECL imaging system is luminol (5-amino-2, 3-dihydro-1,4-phthalazinedione) which reacts with hydrogen peroxide to produce light. The luminescence is positively dependent on the amount of hydrogen peroxide, and thus, this imaging system attracts the interest for bioanalytical applications in the context of detection of reactive oxygen species and oxidative stress. In addition, it allows monitoring the enzymatic activity of oxidases which generate hydrogen peroxide in presence of their substrate.

ECL mechanism depends on numerous experimental parameters: electrode material, solvent, pH, presence of surfactant, respective concentrations of the co-reactant and of the ruthenium complex, hydrophobicity of the electrode surface, etc. The different competitive mechanistic pathways of  $[\text{Ru}(\text{bpy})_3]^{2+}$ /TPrA couple for ECL imaging can be classified into two main groups depending on how

$[\text{Ru}(\text{bpy})_3]^{2+}$  is oxidized. The first “direct” route, as demonstrated in Figure 1A, requires the direct oxidation of the ruthenium complex at the electrode surface to generate ECL. However, these mechanistic routes cannot account for the ECL imaging reported at low oxidation potentials and also for the excellent sensitivity of the bead-based immunoassays. A second “revisited” route involving the diffusing TPrA radicals, as shown in Figure 1B, explains how ruthenium complexes located at micrometric distances from the electrode surface produce ECL.<sup>27</sup> In this mechanism, only the co-reactant TPrA is oxidized at the electrode and the resulting radicals,  $\text{TPrA}^{\bullet+}$  and  $\text{TPrA}^\bullet$ , diffuse and react with the luminophore to generate an excited state and photon emission ( $\sim 615$  nm).<sup>28,29</sup> ECL of this system is obtained at physiological pH and the luminophore is regenerated during the process.

Different mechanisms about luminol/hydrogen peroxide system have been proposed depending on the applied potentials and the experimental conditions.<sup>30-32</sup> Classically, luminol deprotonates in basic solution to form an anion that is first oxidized to a diazaquinone form and the ensuing 3-aminophthalate in the excited state at the electrode surface. This latter decay to the ground state and emits typical light at 425 nm. Dedicated to the imaging in neutral solution for bioanalysis, a luminol analog, 8-amino-5-chloro-7-phenylpyrido [3,4-d]pyridazine-1,4 (2H,3H) dione sodium salt (L012), is frequently used, because this anion can be electrochemically oxidized and emit much stronger luminescence than luminol, as displayed in Figure 1C. With a co-reactant such as hydrogen peroxide, oxygen radicals are electrochemically produced at the electrode and accelerate the generation of the excited 3-aminophthalate for enhanced ECL. In this system, luminol undergoes an irreversible oxidation, which means that it can produce photon just once in the process and not electrocatalytically as the  $[\text{Ru}(\text{bpy})_3]^{2+}$  luminophore. On the other hand, luminol ECL requires a lower anodic potential (i.e.  $\sim 0.4$  V) than  $[\text{Ru}(\text{bpy})_3]^{2+}$ , which is favorable for the imaging of living cells.

## 2.2 Apparatus for ECL imaging

Since no excitation light is involved, the setup of ECL imaging is relative simple and can be adjusted based on the applications. Figure 1D shows the schematic illustration of a basic ECL imaging setup, which is assembled with a simple bright field microscopy, an electrochemistry module (including a cell and a potential generator) and a charge coupled device (CCD) recording the image. The typical electrochemical module is based on a classical two or three-electrode system applied with a direct current (DC) potential.<sup>33</sup> Many well-developed potential protocols to boost the electrochemical property of the electrode surface or generate more radicals in the electrochemical process have been adopted for enhanced luminescence during the imaging. We proposed, a periodic switching between positive and negative potential applied at indium tin oxide (ITO) slides was hypothesized to minimize the metallic surface passivation and provide stronger luminescence from luminol/hydrogen peroxide system.<sup>34</sup> Also, a bi-potentiostatic mode was exerted on two pieces of ITO slides that were assembled in a thin-layer cell, in which one piece was in charge of yielding

enough oxygen radicals under low potential and another boosted the oxidative intermediate of luminol under high potential.<sup>35</sup> As a result, a stronger and constant ECL intensity was obtained through energy transfer between those active species. Furthermore, an alternating current (AC) potential was introduced at the electrode surface to produce the reversible switched bias polarity between anode and cathode. The generation of oxidized and reduced species at the same electrode surface resulted in the efficient generation of annihilation ECL without long-distance diffusion of the relevant species providing a high-intensity emission.<sup>36</sup>

An objective with a high numerical aperture (N.A.) to increase the collecting efficiency and a high sensitive CCD camera to enable single photon detection are two other critical components for high spatial resolution ECL imaging. Due to the weak luminescence generated, the spatial resolution can be compromised by the magnification of the object and the smallest size generating a measurable luminescence. It is noted that, if the luminophore is not attached to the sample, the ECL intermediates could be present in microseconds during this process. This diffusion of these species induces the delocalization between the bright-field and ECL images affecting the spatial resolution of ECL image.<sup>34</sup> Therefore, the current spatial resolution of ECL imaging is restricted to a few micrometer, and the achievement of nanometer resolution imaging is still challenging.

For the visual detection of bio-molecules that does not need the spatial distinction, a simple CCD or even a mobile phone camera is sufficient to image the luminescence. By analyzing the pixel intensity in the digital ECL image, di-n-butylaminoethanol (DBAE) as low as 250  $\mu\text{M}$  was detected using the mobile camera.<sup>37,38</sup> Most importantly, as compared with high sensitive CCD with two colors only, the digital camera has the inherent color selectivity that could be applied to exploit the distinct excitation and emission properties of concomitant ECL. This feature permits multiplexed ECL detection for the development of low-cost and portable clinical diagnostic devices.<sup>39</sup>

### **3. ECL imaging at wired and wireless electrodes for bioanalysis.**

#### **3.1 Wired electrodes**

The ECL signal depends directly on the concentration of the luminophore as well as of the co-reactant. Therefore, both can be potentially detected and quantified as their concentrations directly influence ECL intensity. It allows exploiting various types of biomolecular interactions for the specific detection of targeted analytes of biological interest such as, for example, enzymatic substrates, proteins, and nucleic acids. In addition, ECL as an imaging readout mechanism may resolve spatially the light distribution from different ROIs at the electrode. Thus the ECL imaging method enables multiplexed assays because all the individual spots in an array are simultaneously imaged.

Enzymatic activities of both oxidase and dehydrogenase-type enzymes are measured by ECL using luminol and  $[\text{Ru}(\text{bpy})_3]^{2+}$ , respectively. On one hand, luminol reacts with hydrogen peroxide produced by the oxidase enzymes and thus the corresponding enzymatic substrates are detected. On

the other hand, NADH-dependent dehydrogenase processes have been measured by ECL because the NADH coenzyme contains an amine group. Therefore it can act as a co-reactant with  $[\text{Ru}(\text{bpy})_3]^{2+}$  and produces ECL whereas  $\text{NAD}^+$  does not behave as a co-reactant. Enzymatic arrays were constructed by the immobilization of different corresponding oxidases in hybrid materials of chitosan and MWCNTs on ITO electrodes. Simultaneous measurements of glucose, lactate and choline at different concentrations were performed by analyzing the luminescence intensities of ECL images (Figure 2A)<sup>40</sup>. These enzymes could be co-included in a photopolymer of sepharose beads charged with the different enzymes and of luminol supporting beads.<sup>41</sup> The particular performances of each biosensing spots (choline, glucose, glutamate, lactate, lysine and uric acid) were measured with equivalent analytical performances in comparison to mono-enzymatic detection without a significant cross reactivity.

Our group fabricated nanoneedle electrodes that could generate visible ECL at the nanometer-sized tip through enhanced mass transfer of luminophore and/or co-reactants at the tip.<sup>42,43</sup> Glucose oxidase was embedded in the Nafion coated electrode surface and the generated ECL intensity of all the nanoneedles was mapped. The concentration of glucose ranging from 0.5 to 5 mM was quantified that demonstrated a very high-density (over  $4 \times 10^3$  spots/ $\text{mm}^2$ ) electrochemical analysis (Figure 2B).<sup>43</sup>

The sensitive detection of biomarker proteins is of fundamental importance for early diagnostics and therapy monitoring. Currently, a large number of immunoassays are commercialized for cardiac and infectious diseases, thyroid and tumor markers, etc. ECL imaging has been exploited by Rusling et al. in an array format to detect two cancer biomarker proteins (IL-6 and PSA) in patient sera.<sup>44</sup> Their approach involved microwells incorporating antibody-coated SWCNT forests surrounded by hydrophobic polymer walls. Such nanostructured electrode surfaces provided high functionalized surface areas for the attachment of large populations of capture antibodies in sandwich immunoassays. In addition, silica nanoparticles containing  $[\text{Ru}(\text{bpy})_3]^{2+}$  were employed to enhance the ECL signals. The detection limits for IL-6 and PSA were equivalent to or better than commercial bead-based protein measurement systems. The spatial distribution of ECL-active sites of the array in ECL imaging present a significant advantage over voltammetric arrays in that individual electrical connections to the individual wells or spots are not necessary. This approach has been extended for the detection of 4 proteins with microfluidic channels.<sup>45</sup>

Genotoxicity screening was also reported using ECL imaging of array spots containing DNA, various isoforms of cytochrome P450, and ECL-active metallopolymer  $[\text{Ru}(\text{bpy})_2\text{PVP}_{10}]^{2+}$  (Figure 2C).<sup>46</sup> The thin-film spots were exposed to hydrogen peroxide to activate the enzymes, which generate metabolites. Several human isoforms of cytochrome P450 were simultaneously tested for their activity toward the procarcinogen benzo[a]pyrene. Up to 50 distinct enzyme/DNA spots in an array were simultaneously imaged allowing to estimate relative rates of DNA damage associated with

the enzymes. Relative genotoxicity from bioactivated metabolites is thus assigned to specific enzymes.

Various amplification strategies are designed and implemented in ECL immunosensor arrays. These strategies are essential in ECL imaging to increase the signal-to-noise ratio (contrast) in the images. For example, the ECL intensity was enhanced by associating polymer dots and a dual DNA amplification strategy.<sup>47</sup> It was achieved on the immunoarrays by rolling circle amplification of oligonucleotide strands and then enzymatically cyclic release of polymer dots from self-quenched probes. The polymer dots showed 11 times higher ECL efficiency than previously reported systems, and the deposition of gold on ITO enhanced the ECL signal by 100-fold. In addition, the high quenching efficiency of black hole quencher provided low background for “off-on” imaging.

Su et al. reported a very original application of ECL imaging by visualizing latent fingerprints in both negative and positive modes.<sup>48</sup> In the negative-imaging mode, the ITO electrode bearing a sebaceous (sebum-rich) fingerprint make the underlying surface ECL inert or less active. Thus, the ECL emission was generated mainly from the bare surface in presence of TPrA. This mode does not involve any pre-/post-treatment, which is usually laborious and requires in most of current detection methods. In the positive mode, the fingerprint ridge deposit was tagged with a ruthenium derivative. These immobilized ECL-generating luminophores react with freely diffusing co-reactants to generate locally ECL. This strategy was further extended to the immuno-imaging of secretions in human perspiration present in latent fingerprints using horseradish peroxidase and luminol as labels and luminophores, respectively.<sup>49</sup> Figure 2D shows an ECL image of an human immunoglobulin G (hIgG) groomed fingermark. This ECL imaging approach enables both identification of an individual and recognition of the secretions in the human perspiration.

### 3.2 Wireless electrodes

Bipolar electrochemistry (BPE) is an electrochemical approach based on the polarization of a conducting object placed in an electric field, which generates the potential difference between the two extremities. With sufficient potential difference, opposite redox reactions are triggered at these two extremities.<sup>50,51</sup> Since Fleischmann et al. demonstrated the water splitting using bipolar microelectrodes, multiple applications in the fields of sensors, electrocatalyst, fluorescence, material enrichment and separation have been developed.<sup>52</sup> The attractive feature of bipolar electrodes is the absence of the connection of the electrode with the external power, which facilitates electrochemistry to be carried out on the microelectrodes.

The first combination of ECL with BPE in a microfluidic system by Manz et al. in 2001.<sup>53</sup> In the next year, Crooks et al. improved the detection principle and used the anodic reaction solely as an ECL reporter of events occurring at the cathode.<sup>54</sup> Accordingly, the electrochemical reduction of the analyte, benzyl viologen ( $BV^{2+}$ ), could be indicated by the luminescence intensity from the oxidation

of  $\text{Ru}(\text{bpy})_3^{2+}$  in presence of TPrA. The successful coupling of ECL and BPE provides a convenient and sensitive means for direct photonic readout of electrochemical reactions.

Taking the advantage of ECL imaging, a current flowing in multiple bipolar electrodes is observed as light emission simultaneously. In the first work, an electrochemical DNA microarray was fabricated within a microfluidic channel as an “open” BPE system.<sup>55</sup> The interfacial potential of multiple, well-defined bipolar electrodes were controlled by two wires regardless of the electrode number (Figure 3A). By measuring the luminescence intensity in the image, the hybridization of DNA oligonucleotides was sensed at the array.<sup>56</sup> The current electrode density in the array for ECL imaging was reported to be  $\sim 2000$  sensing elements/ $\text{cm}^2$ , which was comparable to the typical density for a fluorescence-based microarray.<sup>57</sup>

The physical separation of the ECL reporting cocktail and the solution containing the target is important to prevent chemical interferences between the two extremities. To address this issue, a two-channel microelectrochemical sensor that communicates between separate sensing and reporting microchannels via one or more BPEs was designed as the “closed” BPE system. When the sensing pole was activated by a target, ECL was emitted at the reporting pole.<sup>58</sup> ECL signal obtained at the anode of bipolar electrode in the closed BPE was observed to be much stronger than that in the open BPE, confirming the enhanced potential difference between solution/BPE interface in the closed BPE. To expand the application range of the  $[\text{Ru}(\text{bpy})_3]^{2+}$ -TPrA anodic ECL reaction, the three-channel and BPE configuration was designed to include all the oxidants, reductants, or chemicals so that all of them can be detected in a single device.<sup>59</sup>

Biorecognition elements (aptamer or antibody) and a probe (e.g. thionine) can be immobilized at the cathodes by the recognition of different target analytes. In presence of more analytes, the electrochemical conversion of thionine increases, enhancing the ECL signals due to the charge neutrality of bipolar electrode. As a result, multiplex detection of cancer biomarkers was realized on the cathodic poles of BPEs that was reported in the ECL images.<sup>60</sup> The gap between the two ITO bands could be regarded as an electrical switch, the conductivity of which were regulated by the protein (e.g. prostate cancer antigen, PSA) guided silver particles. In this strategy, an electronic circuit between the adjacent BPEs was achieved by the deposition of silver particles in presence of PSA. Accordingly, a sensitive visual measurement of PSA was realized by the imaging of ECL at BPE (Figure 3C).<sup>61</sup>

In the previous examples, the multiplexing capabilities of ECL imaging rely mainly on the fabrication of arrays of sensing spots. But the performances may be improved by tuning the ECL emission colors. Indeed, multiple, spectrally distinct ECL luminophores add a new dimension for multi-analyte imaging and increase the complexity of the analytical platforms.<sup>62,63</sup> Bidirectional color change from blue-green to red was observed by selective excitation of iridium and ruthenium complexes by scanning the electrode potential.<sup>64,65</sup> Imaging the color switching from blue-green to

red enabled the measurement of multiple prostate cancer biomarkers (PSA, circulating microRNA-141, and sarcosine) (Figure 3D).<sup>66</sup> Such array platforms using enzymes or proteins show the interest of performing highly multiplexed assays using ECL imaging.

Both wireless features and asymmetric redox reactivity of BPE is exploited, which offers the possibility to design analytical ECL swimmers. The application of an electric field across the solution promoted simultaneous reduction of O<sub>2</sub> at the cathodic pole of a conductive bead and oxidation of ECL reagents at its anodic pole. Thus it induced both motion and ECL-light emission from the bead in a capillary.<sup>67,68</sup> In this case, ECL imaging provides a direct monitoring of the swimmer motion, which could be very useful for localizing micromotors. An analytical task was also associated to such ECL swimmers to explore and report the local glucose concentration by combining it with an enzymatic reaction.<sup>69</sup> Glucose dehydrogenase oxidized glucose to gluconolactone with the concomitant conversion of NAD<sup>+</sup> to NADH, which acted as a co-reactant in the ECL process. The simultaneous oxidation of the luminophore and of the enzymatically-produced NADH led to ECL emission with a glucose-dependent light intensity. A concentration gradient of glucose was explored by the ECL swimmer and, as it was moving towards a region of higher glucose concentration, its ECL intensity increased. Thus ECL allowed to visualize and measure remotely the local concentration of the enzymatic substrates.<sup>70</sup> This concept was later extended to 3D ECL by generating light at the level of millions of micro-emitters dispersed in solution.<sup>70,71</sup> Each single object was addressed remotely by BPE and they generate collectively the luminescence in the bulk. Therefore, the entire volume of the solution produces light and ECL imaging was used as a readout method to visualize the concentration gradients in a single ECL image.

#### **4. ECL imaging of single objects.**

##### **4.1 Single cells.**

High throughput and spatial/temporal analysis at single living cells provide valuable information about the cell features that are associated with cellular heterogeneity. Although fluorescence imaging is popular to investigate the distribution and content of bio-molecules, the design and synthesis of specific fluorescence probe for small molecules are time-consuming, and the specificities of these probes often subject to caution. Moreover, high background signal in fluorescence image of cells is defavorable to visualize low-content membrane proteins. While, ECL imaging involves commercially available oxidases to react with the corresponding small molecules generating hydrogen peroxide. Hydrogen peroxide produced enhances ECL from aqueous luminol and the luminescence intensity is proved to be correlated with the amount of target molecules.<sup>72,73</sup> The detection strategy is illustrated in Figure 4A. More importantly, ECL imaging could efficiently minimize the background signals for the sensitive measurement of small molecules and membrane proteins at cells.<sup>1,74</sup>

To perform single cell ECL imaging, cell-sized microwells were fabricated at ITO slides to retain individual living cells. Visible ECL from luminol and hydrogen peroxide were imaged at bare ITO regions in the microwells. The modification of g-C<sub>3</sub>N<sub>4</sub> nanosheets at ITO regions catalyzed the decomposition of hydrogen peroxide resulting in more •OH radical and enhanced ECL.<sup>75</sup> Accordingly, the lowest visualized concentration reported by our group was 500 nM that guaranteed the detection of low concentrated cholesterol at single cells in parallel. During single cell imaging, the consumption of membrane molecules by oxidases was completed in a few minutes. The continuous generation of hydrogen peroxide from cellular surface and the escape (free diffusion) of hydrogen peroxide from the microwells to the bulk solution are proved to offer a near steady-state concentration at bare ITO regions in a certain time period.<sup>73</sup> By recording the luminescence in this period (Figure 4B), membrane cholesterol at 64 cells was quantified and a heterogeneity as high as 35.7% for cholesterol content was observed exhibiting the significance of single cell analysis.

The expansion of single cell ECL imaging to intracellular analysis is challenging, but important, for the biological study because the cellular activity is strongly associated with the fluctuation of intracellular molecule amount. Triton X-100 was co-added with oxidase to break plasma membrane of individual cells in the microwells. The intracellular molecules, such as glucose and cholesterol ester, were released and then reacted with the oxidases to generate hydrogen peroxide in the microwell.<sup>76</sup> The luminescence from 64 individual cells on one ITO slide was visualized, which enlightens the feasibility of intracellular ECL imaging at single cells. Further evidence exhibited that the removal of membrane cholesterol by cholesterol oxidase maintained the cellular membrane intact.<sup>77</sup> Therefore, the same individual cells could be exposed to different oxidases in multiple steps providing the images of membrane and intracellular cholesterol.<sup>75</sup> This co-detection of multiple molecules should offer more information for the study of cholesterol-related pathways at single cells.

Although single cell imaging by ECL could provide high-through analysis, applying this technique for clinic tests requires simple fabrication of the chips. Currently, multiple-step fabrication of photoresist based microwells involving the coating and partial removal of photoresist from ITO slide is well-developed, but still complicated. A simple protocol using a silica stamp was developed to prepare PDMS microwells that take place of the previous photo-resist microwells.<sup>78</sup> After a simple spraying of an Au layer on the PDMS chip, a clean conductive surface was produced to induce higher luminescence intensity for single cell glucose analysis. This two-step fabrication does not involve the exposure and washing process that simplifies the chip production.

Another technical goal of single cell ECL imaging is to obtain high spatial (nanometer level) and temporal (millisecond level) measurement at one cell so that the subtle information associated with the cellular activity could be monitored without any labeling. The tentative work was conducted to image the efflux of hydrogen peroxide from single living cells.<sup>34</sup> When the cells were cultured in the physiological buffer with luminol, the existence of membrane ruffling created small space between the

lower surface of the cell and ITO slide retaining some amount of luminol. Under the electrochemical control, the released hydrogen peroxide reacted with luminol in these spaces emitting the luminescence so that the efflux of hydrogen peroxide beneath the cell was imaged (Figure 4C). The addition of cholesterol oxidase into the buffer generated hydrogen peroxide from the reaction with membrane cholesterol, and thus, offered ECL images of cholesterol distribution at the cellular surface. However, the limited amount of luminol beneath the cells and the steric hindrance of luminol from the solution to these space restrict the luminescence at the cells affecting the quality of ECL image. The introduction of permeable chitosan film at ITO slides increased the space between the cells and the electrode surface. Consequently, more luminol was present below the cells, which improved the sensitivity of single cell imaging.<sup>79</sup>

Despite that the efflux of hydrogen peroxide and the distribution of membrane cholesterol are imaged, the diffusion of these ECL intermediates is unavoidable affecting the spatial characterization. Our result showed  $\sim 2 \mu\text{m}$  blurry luminescence edge surrounding the cells that revealed the existence of lateral diffusion.<sup>34</sup> Therefore, the diffusion of these species limits the spatial resolution of ECL imaging with a few micrometers. An alternative strategy to achieve the local imaging of cellular information might be the usage of micro/nano-tips in ECL imaging. Our group fabricated a comprehensive Au-luminol- microelectrode that was inserted into the cell. The bright luminescence observed at the tip visualized local concentration of hydrogen peroxide inside the cells (Figure 4D).<sup>80</sup>

Besides small molecules in the cells, membrane proteins at single cells were imaged using ECL as a surface-confined microscopy.<sup>81</sup> By contrast with classic fluorescence microscopy, ECL emission was only detected from the  $[\text{Ru}(\text{bpy})_3]^{2+}$  labels immobilized on the cell membrane located in the immediate vicinity of the electrode surface (Figure 4E). This result is intrinsically associated to the unique ECL mechanism of TPrA due to the limited lifetimes of the electrogenerated TPrA radicals (Figure 1B). The potential diagnostic applications of this approach were reported by using carbon nanotubes (CNT)-based inkjet-printed disposable electrodes for the direct ECL imaging of a labeled plasma receptor over-expressed on tumor cells. The ECL luminophore was linked to an antibody targeting an important membrane receptor, the epidermal growth factor receptor (EGFR), which was a plasma membrane receptor over-expressed in several cancer cells. This important work allows the development of new surface-confined microscopy and of ultrasensitive single cell imaging assays. To improve the ECL imaging sensitivity of tumor markers expressed at the cell level, BPE and functional nanoprobe of heterogeneous  $[\text{Ru}(\text{bpy})_3]^{2+}@\text{SiO}_2/\text{Au}$  nanoparticles were combined for visual immunoassay of prostate specific antigen (PSA) at single cells.<sup>82</sup> Such silica NPs enabled the immobilization of a large amount of labels, and the Au NPs decorated on the surface of  $[\text{Ru}(\text{bpy})_3]^{2+}@\text{SiO}_2$  NPs increased the amount of loaded antibody so that more luminescence was obtained.

## 4.2 Single particles

Micro/nano-particles with high electron-transfer rate and electrocatalytic features are being incorporated as the new electrode materials for basic electron-transfer study, electrochemical sensing and electrocatalysis. The examination at the single particle level should contribute to elucidate the correlation between the particle structure and function.<sup>83,84</sup> Due to the challenge of separating the signal at an individual particle from the surrounding particles and/or environment, single particle electrochemistry is combined with optical techniques providing a solution to image electrochemical signal at multiple particles in parallel. Since ECL has near-zero background readout and the corresponding high-sensitivity, single particles ECL imaging becomes a highly promising tool in this field.

The pioneering work on single-nanoparticle ECL analysis was conducted by the group of Bard. They immobilized sub-25 nm single polymer nanoparticles at ITO slides and observed ECL from single particles in the presence of a co-reactant. The ECL photons as high as 1500 photons during 100 s from individual nanoparticles exhibits the feasibility of this technique for the bio-sensing.<sup>85,86</sup> The early work of single particle ECL imaging for biosensing was realized at  $\sim 3.1 \mu\text{m}$  polystyrene microbeads modified with antigens.<sup>27</sup> Upon the recognition by  $[\text{Ru}(\text{bpy})_3]^{2+}$  tagged antibodies, the visual luminescence emitted from the entire bead demonstrated the possibility of performing multiplexed immunoassays using ECL imaging (Figure 5A). The possibility of performing highly multiplexed assays by ECL was demonstrated because all the individual sensing beads in the array were simultaneously imaged and individually resolved by ECL. Such a three electrode configuration for ECL imaging was continuously optimized using  $8 \mu\text{m}$  polystyrene beads coated with a  $\text{Ru}(\text{bpy})_3^{2+}$  complex.<sup>87</sup> The concentration of  $\text{Ru}(\text{bpy})_3^{2+}$  complex as low as  $1 \times 10^{-19} \text{ mol}/\mu\text{m}^2$  at the microbeads could be imaged.

Furthermore, single particle ECL imaging was also achieved to visualize electrocatalytic reaction activity at single quantum dots (QDs) loaded silica microparticle involved in water oxidation.<sup>88</sup> Under anodic voltage, the active redox centers at CdSeTe QDs induced the generation of hydroperoxide surface intermediates as co-reactants to remarkably enhance ECL emission from luminol for imaging (Figure 5B). A linear relation between ECL intensity and turn over frequency suggests that ECL intensity can be used as a visual signal to exhibit the electrocatalytic activity of single particles. A quasi-zero background luminescence is obtained in the full potential window, which is advantageous versus the other optical imaging with the fluctuation of background signal under high voltage.

To realize ECL imaging of single nanoparticles (NPs), the metal materials have received attention due to their good ability for reaction catalysis and electron transfer, and good biocompatibility. Au nanoparticles could catalyze the oxidation of TPA to enhance ECL from  $\text{Ru}(\text{bpy})_3^{2+}$ . As a result, the luminescence from single Au NPs was firstly imaged (Figure 5C).<sup>89</sup> The luminescence intensity at individual nanoparticles was positively dependent on the particle size from 30 to 300 nm, and was

affected by the local chemical and charge transfer environment of the NPs. The achievement should permit a massively parallel direct readout of local redox activities on single nanoparticles. However, the obtained ECL from single NPs was vanished within several seconds because of the surface oxidation of Au NPs. To overcome the surface oxidation of Au NPs in aqueous environments, a polymer blend was coated at single Au nanowires resulting in readily measurable ECL.<sup>90</sup> ECL image quality and reproducibility over multiple redox cycles could be improved with thicker polymer layer.

Recently, Au-Pt Janus NPs, meaning particles with different surfaces or asymmetric reactivity, were prepared exhibiting enhanced ECL intensity and stability.<sup>91</sup> Different heterogeneous electron-transfer rate constants at Au and Pt results in a concentration difference arose at the asymmetric bimetallic interface. The fluid slip around the Janus particle enhanced local redox reactions and protected the particle surface from passivation. Therefore, in comparison to the monometal NPs, the Janus particles weakened the surface poisoning and exhibited much better long-time stability that improved the quality of ECL imaging significantly.

Single-particle collision is another exciting direction to examine the electrochemical features of individual NPs, which takes place on a macroscopic electrode at exceedingly high frequencies. Classically, single particle events can be temporally resolved using a microelectrode as the recording electrode. The combination of ECL imaging and single-particle collision should help to investigate the dynamic redox behavior of multiple NPs at the electrode/solution interface for more detail information. To achieve this aim, ECL imaging with sufficient spatial and temporal resolutions is critical to track the fast diffusional motion of the NPs at the interface. The currently fastest temporal resolution of ECL imaging was reported to be 200 ms from the imaging of  $\sim 62$  nm Ru(bpy)<sub>3</sub><sup>2+</sup> doping silica nanoparticles.<sup>92</sup> Several discrete ECL spots were observed successively in different ROIs, which provided the direct evidence for the ECL visualization of collision electrochemistry (Figure 5D). Two major categories “spike” and “staircase”, of the ECL signals from the nanoparticles suggest the elastic and sticking collision, respectively.

## 5. Remarks

The electrochemical mapping of the distribution of bio-molecules at heterogeneous and microscopic interfaces is significant for high spatio-temporal bioanalysis. SECM is a classic approach to obtain spatially resolved electrochemical signals. However, due to the use of scanning electrodes, high temporal resolution is not realized. Plasmonic-based electrochemical microscopy allows wide-field imaging of the interfacial distribution of an electrochemical signal from a planar electrode with simultaneous submicron spatial resolution and sub-millisecond temporal resolution, but the sensitivity is being improved. ECL imaging is a fast-developing technology that owes the advantages of high detection sensitivity and spatial/temporal resolutions in bioanalysis. Various electrode materials and

architectures, and imaging strategies have been realized to achieve lower detection limits, better resolutions and image quality.

Despite the successes of ECL imaging, many challenging, such as single molecule detection, super-resolution imaging and the application in clinic test, are present in the field of ECL imaging. The modern biological study has revealed that many biological events at single molecule level occur at nanometer sized region in nanoseconds. To fulfill the requirement, a series of revolutionary developments in fluorescence microscopy have circumvented the limit of light diffraction and provided an image of single molecules with subcellular spatial resolution below 200 nm. However, the current detection limit and the spatial/temporal resolutions in ECL imaging are far less than the biological requirements that need the breakthrough in the detection principle, setup and strategy.

The performances of the ECL imaging depends on several factors related directly to the ECL process such as the sensing strategies, the efficiency of the ECL generation, the ECL mechanisms of the luminophores and the co-reactants as well as the optical detection. Therefore, the endeavor to prepare novel electrodes with higher electron transfer rate and luminophores with high luminescence efficiency should be targeted to obtain significant enhancement in ECL signals. And, the optical detection relies on the instrumentation and the optical components (objectives, 2D photodetectors, etc.) and ECL imaging should benefit also from the fast progresses in the microscopy field. Moreover, imaging the ECL reactivity on single objects should provide insights into the ECL mechanistic routes allowing to select new co-reactants and luminophores with improved sensitivity and to develop new imaging strategies. As already mentioned, two co-reactant ECL systems ( $[\text{Ru}(\text{bpy})_3]^{2+}/\text{TPA}$  and luminol/ $\text{H}_2\text{O}_2$ ) are mainly used for imaging purposes. However, the developments of original strategies by combining ECL with wireless addressing methods and by using multicolor ECL emission and nanoluminophores such as QDs or doped nanoparticles open new avenues to develop original ECL-based microscopies.

In addition, the current co-reactant ECL is commercialized for more than 100 immunoassays, which are vital for early diagnosis and treatments of the corresponding pathologies. The continuous coupling of ECL imaging strategies and these immunoassays offers exciting opportunities and promising applications in ultrasensitive ECL-based imaging assays for clinic test.

#### **Disclosure statement.**

The authors are not aware of any affiliations, memberships, funding, or financial holdings that might be perceived as affecting the objectivity of this review.

#### **Acknowledgements.**

We apologize in advance to all the investigators whose research could not be cited due to space limitations. We are grateful for financial support from the National Natural Science Foundation of

China (grants 21327902 and 21575060) and from the Agence Nationale de la Recherche (NEOCASTIP ANR-15-CE09-0015-03).

#### Literature cited.

1. Richter MM. 2004. Electrochemiluminescence (ECL). *Chem. Rev.* 104:3003-6
2. Miao WJ. 2008. Electrogenerated chemiluminescence and its biorelated applications. *Chem. Rev.* 108:2506-53
3. Santhanam KSV, Bard AJ. 1965. Chemiluminescence of electrogenerated 9,10-diphenylanthracene anion radical<sup>1</sup>. *J. Am. Chem. Soc.* 87:139-40
4. Short GD, Hercules DM. 1965. Electroluminescence of organic compounds. The role of gaseous discharge in the excitation process. *J. Am. Chem. Soc.* 87:1439-42
5. Bard AJ. 2004. *Electrogenerated Chemiluminescence*. New York: Marcel Dekker.
6. Bard AJ. 2014. A life in electrochemistry. 7:1-21
7. Forster RJ, Bertonecello P, Keyes, TE. 2009. Electrogenerated chemiluminescence. *Annu Rev Anal Chem.* 2:359-85
8. Valenti G, Fiorani A, Li H, Sojic N, Paolucci F. 2016. Essential role of electrode materials in electrochemiluminescence applications. *Chem Electro Chem.* 3:1990-7
9. Engstrom RC, Johnson KW, DesJarlais S. 1987. Characterization of electrode heterogeneity with electrogenerated chemiluminescence. *Anal. Chem.* 59:670-3
10. Engstrom RC, Pharr CM, Koppang MD. 1987. Visualization of the edge effect with electrogenerated chemiluminescence. *J. Electroanal. Chem.* 221:251-5
11. Bowling RJ, McCreery RL, Pharr CM, Engstrom RC. 1989. Observation of kinetic heterogeneity on highly ordered pyrolytic graphite using electrogenerated chemiluminescence. *Anal. Chem.* 61:2763-6
12. Pharr CM, Engstrom RC, Klanke J, Unzelman PL. 1990. Determination of microscopic electrode kinetics with electrogenerated chemiluminescence imaging. *Electroanalysis.* 2:217-21
13. Amatore C, Pebay C, Servant L, Sojic N, Szunerits S, et al. 2006. Mapping electrochemiluminescence as generated at double-band microelectrodes by confocal microscopy under steady state. *ChemPhysChem.* 7:1322-7
14. Szunerits S, Tam JM, Thouin L, Amatore C, Walt DR. 2003. Spatially resolved electrochemiluminescence on an array of electrode tips. *Anal Chem.* 75:4382-8
15. Chovin A, Garrigue P, Vinatier P, Sojic N. 2004. Development of an ordered array of optoelectrochemical individually readable sensors with submicrometer dimensions: application to remote electrochemiluminescence imaging. *Anal. Chem.* 76:357-64
16. Chovin A, Garrigue P, Sojic N. 2006. Remote NADH imaging through an ordered array of electrochemiluminescent nanoapertures. *Bioelectrochemistry.* 69:25-33

17. Bard AJ, Fan FRF, Kwak J, Lev O. 1989. Scanning electrochemical microscopy. Introduction and principles. *Anal. Chem.* 61:132-8
18. Amemiya S, Bard AJ, Fan FRF, Mirkin MV, Unwin PR. 2008. Scanning electrochemical microscopy. *Annu Rev Anal Chem.* 1:95-131
19. Hansma PK, Drake B, Marti O, Gould SAC, Prater CB. 1989. The scanning ion-conductance microscope. *Science.* 243:641-3
20. Chen CC, Zhou Y, Baker LA. 2012. Scanning ion conductance microscopy. *Annu Rev Anal Chem.* 5:207-28
21. Hercules DM. 1964. Chemiluminescence resulting from electrochemically generated species. *Science.* 145:808-9
22. Visco RE, Chandross EA. 1964. Electroluminescence in solutions of aromatic hydrocarbons. *J. Am. Chem. Soc.* 86:5350-1
23. Santhanam KSV, Bard AJ. 1965. Chemiluminescence of electrogenerated 9,10-diphenylanthracene anion radical. *J. Am. Chem. Soc.* 87:139-40
24. Rubinstein I, Bard AJ. 1981. Electrogenerated chemiluminescence. 37. Aqueous ECL systems based on tris(2,2'-bipyridine)ruthenium(2+) and oxalate or organic acids. *J. Am. Chem. Soc.* 103:512-6
25. Noddsinger JB, Danielson N. 1987. Generation of chemiluminescence upon reaction of aliphatic amines with tris(2,2'-bipyridine)ruthenium(III). *Anal. Chem.* 59:865-8
26. Leland JK, Powell MJ. 1990. Electrogenerated chemiluminescence: an oxidative-reduction type ECL reaction sequence using tripropyl amine. *J. Electrochem. Soc.* 137:3127-31
27. Deiss F, LaFratta CN, Symer M, Blicharz TM, Sojic N, Walt DR. 2009. Multiplexed sandwich immunoassays using electrochemiluminescence imaging resolved at the single bead level. *J. Am. Chem. Soc.* 131:6088-9
28. Miao WJ, Choi J, Bard AJ. 2002. Electrogenerated chemiluminescence 69: the Tris(2,2'-bipyridine)ruthenium(II),(Ru(bpy)<sub>3</sub><sup>2+</sup>)/Tri-*n*-propylamine (TPrA) system revisited-A new route involving TPrA<sup>+</sup> cation radicals. *J. Am. Chem. Soc.* 124:14478-85
29. Sentic M, Milutinovic M, Kanoufi F, Manojlovic D, Arbault S, et al. 2014. Mapping electrogenerated chemiluminescence reactivity in space: mechanistic insight into model systems used in immunoassays. *Chem. Sci.* 5:2568-72
30. Sakura S. 1992. Electrochemiluminescence of hydrogen peroxide-luminol at a carbon electrode. *Anal. Chim. Acta.* 262:49-57
31. Lin XQ, Sun YG, Cui H. 1999. Potential-resolved electrochemiluminescence of luminol in alkaline solutions at glassy carbon and platinum electrodes. *Chinese J. Anal. Chem.* 27:502-3
32. Cui H, Xu Y, Zhang Z. F. 2004, Multi-channel electrochemiluminescence of luminol in neutral and alkaline aqueous solutions on a gold nanoparticles self-assembled electrode. *Anal. Chem.* 76:

4002-4010.

33. Yamazaki-Nishida S, Harima Y, Yamashita K. 1990. Direct current electrogenerated chemiluminescence observed with  $[\text{Ru}(\text{bpz})_3^{2+}]$  in fully aqueous solution. *J. Electroanal. Chem.* 283:455-8
34. Zhou JY, Ma GZ, Chen Y, Fang DJ, Jiang DC, et al. 2015. Electrochemiluminescence imaging for parallel single-cell analysis of active membrane cholesterol. *Anal. Chem.* 87:8138-43
35. Ming L, Peng YY, Tu YF. 2014. A new strategy for exciting the electrochemiluminescence of luminol by double-static potential. *Electrochem. Commun.* 46:107-10
36. Eßmann V, Clausmeyera J, Schuhmann W. 2017. Alternating current-bipolar electrochemistry. *Electrochem. Commun.* 75:82-5
37. Hao N, Xiong M, Zhang J.D., Xu J.J., Chen H.Y. 2013. Portable thermo-powered high-throughput visual electrochemiluminescence sensor. *Anal Chem.* 85:11715-9.
38. Delaney JL, Hogan CF, Tian JF, Shen W. 2011. Electrogenerated chemiluminescence detection in paper-based microfluidic sensors. *Anal. Chem.* 83:1300-6
39. Doeven EH, Barbante GJ, Kerr E, Hogan CF, Endler JA, et al. 2014. Red-green-blue electrogenerated chemiluminescence utilizing a digital camera as detector. *Anal. Chem.* 86:2727-32
40. Zhou ZY, Xu LR, Wu SZ, Su B. 2014. A novel biosensor array with a wheel-like pattern for glucose, lactate and choline based on electrochemiluminescence imaging. *Analyst.* 139:4934-9
41. Marquette CA, Degiuli A, Blum LJ. 2003. Electrochemiluminescent biosensors array for the concomitant detection of choline, glucose, glutamate, lactate, lysine and urate. *Biosens. Bioelectronics.* 19:433-9
42. Sentic M, Virgilio F, Zanut A, Manojlovic D, Arbault S, et al. 2016. Microscopic imaging and tuning of electrogenerated chemiluminescence with boron-doped diamond nanoelectrode arrays. *Anal. Bioanal. Chem.* 408:7085-94
43. Zhang JJ, Zhou JY, Tian CX, Yang S, Jiang DC, et al. 2017. Localized electrochemiluminescence from nanoneedle electrodes for very-high-density electrochemical sensing. *Anal. Chem.* 89:11399-404
44. Sardesai NP, Barron JC, Rusling JF. 2011. Carbon nanotube microwell array for sensitive electrochemiluminescent detection of cancer biomarker proteins. *Anal. Chem.* 83:6698-703
45. Kadimisetty K, Malla S, Sardesai NP, Joshi AA, Faria RC, et al. 2015. Automated multiplexed ECL immunoarrays for cancer biomarker proteins. *Anal. Chem.* 87:4472-8
46. Hvastkovs EG, So M, Krishnan S, Bajrami B, Tarun M, et al. 2007. Electrochemiluminescent arrays for cytochrome P450-activated genotoxicity screening. DNA damage from benzo[a]pyrene metabolites. *Anal. Chem.* 79:1897-906
47. Wang NN, Feng YQ, Wang YW, Ju HX, Yan F. 2018. Electrochemiluminescent imaging for

- multi-immunoassay sensitized by dual DNA amplification of polymer dot signal. *Anal. Chem.* 90:7708-14.
48. Xu LR, Li Y, Wu SZ, Liu XH, Su B. 2012. Imaging latent fingerprints by electrochemiluminescence. *Angew. Chem. Int. Ed.* 51:8068-72
  49. Xu LR, Zhou ZY, Zhang CZ, He YY, Su B. 2014. Electrochemiluminescence imaging of latent fingerprints through the immunodetection of secretions in human perspiration. *Chem. Commun.* 50:9097-100
  50. Fosdick SE, Knust KN, Scida K, Crooks RM. 2013. Bipolar electrochemistry. *Angew. Chem. Int. Ed.* 52: 10438-56
  51. Loget G, Kuhn A. 2011. Shaping and exploring the micro-and nanoworld using bipolar electrochemistry. *Anal. Bioanal. Chem.* 400:1691-704
  52. Loget G, Zigah D, Bouffier L, Sojic N, Kuhn A. 2013. Bipolar electrochemistry: from materials science to motion and beyond. *Acc. Chem. Res.* 46:2513-23
  53. Arora A, Eijkel J.C., Morf W.E., Manz A. 2001. A wireless electrochemiluminescence detector applied to direct and indirect detection for electrophoresis on a microfabricated glass device. *Anal. Chem.* 73:3282-8.
  54. Zhan W, Alvarez J, Crooks RM. 2002. Electrochemical sensing in microfluidic systems using electrogenerated chemiluminescence as a photonic reporter of redox reactions. *J. Am. Chem. Soc.* 124:13265-70
  55. Chow KF, Mayre' F, Crooks RM. 2008. Wireless electrochemical DNA microarray sensor. *J. Am. Chem. Soc.* 130:7544-5.
  56. Khoshfetrat SM, Ranjbari M, Shayan M, Kiani A, Kiani A. 2015. Wireless electrochemiluminescence bipolar electrode array for visualized genotyping of single nucleotide polymorphism. *Anal. Chem.* 87:8123-31
  57. Chow KF, Mavré F, Crooks JA, Chang BY, Crooks RM. 2009. A large-scale, wireless electrochemical bipolar electrode microarray. *J. Am. Chem. Soc.* 131:8364-5
  58. Chang BY, Chow KF, Crooks JA, Mavré F, Crooks RM. 2012. Two-channel microelectrochemical bipolar electrode sensor array. *Analyst.* 137:2827-33
  59. Zhang XW, Li J, Jia XF, Li DY, Wang EK. 2014. Full-featured electrochemiluminescence sensing platform based on the multichannel closed bipolar system. *Anal. Chem.* 86:5595-9
  60. Wu MS, Liu Z, Shi HW, Chen HY, Xu JJ. 2014. Visual electrochemiluminescence detection of cancer biomarkers on a closed bipolar electrode array chip. *Anal. Chem.* 87:530-7
  61. Wu MS, Yuan DJ, Xu JJ, Chen HY. 2013. Electrochemiluminescence on bipolar electrodes for visual bioanalysis. *Chem. Sci.* 4:1182-8
  62. Doeven EH, Zammit EM, Barbante GJ, Hogan CF, Barnett NW, et al. 2012. Selective excitation of concomitant electrochemiluminophores: tuning emission color by electrode potential. *Angew.*

*Chem. Int. Ed.* 51:4354-7.

63. Kerr E, Doeven EH, Barbante GJ, Hogan CF, David J, et al. 2015. Annihilation electrogenerated chemiluminescence of mixed metal chelates in solution: modulating emission colour by manipulating the energetics. *Chem. Sci.* 6:472-9
64. Wang YZ, Ji SY, Xu HY, Zhao W, Xu JJ, et al. 2018. Bidirectional electrochemiluminescence color switch: an application in detecting multimarkers of prostate cancer. *Anal. Chem.* 90:3570-5
65. Li HD, Bouffier L, Arbault S, Kuhn A, Hogan C, et al. 2017. Spatially-resolved multicolor bipolar electrochemiluminescence. *Electrochem. Commun.* 77:10-3
66. Wang YZ, Xu CH, Zhao W, Guan QY, Chen HY, et al. 2017. Bipolar electrode based multi-color electrochemiluminescence biosensor. *Anal. Chem.* 89:8050-6
67. Sentic M, Loget G, Manojlovic D, Kuhn A, Sojic N. 2012. Light-emitting electrochemical "Swimmers". *Angew. Chem. Int. Ed.* 51:11284-8
68. Bouffier L, Zigah D, Adam C, Sentic M, Fattah Z, et al. 2014. Lighting up redox propulsion with luminol electrogenerated chemiluminescence. *Chem. Electro. Chem.* 1:95-8
69. Sentic M, Arbault S, Goudeau B, Manojlovic D, Kuhn A, et al. 2014. Electrochemiluminescent swimmers for dynamic enzymatic sensing. *Chem. Commun.* 50:10202-5
70. Sentic M, Arbault S, Bouffier L, Manojlovic D, Kuhn A, et al. 2015. 3D electrogenerated chemiluminescence: from surface-confined reactions to bulk emission. *Chem. Sci.* 6:4433-7
71. Poulpiquet A, Diez-Buitrago B, Milutinovic MD, Sentic M, Arbault S, et al. 2016. Dual enzymatic detection by bulk electrogenerated chemiluminescence. *Anal. Chem.* 88:6585-92
72. Ma GZ, Zhou JY, Tian CX, Jiang DC, Fang DJ, et al. 2013. Luminol electrochemiluminescence for the analysis of active cholesterol at the plasma membrane in single mammalian cells. *Anal. Chem.* 85:3912-7
73. Tian CX, Zhou JY, Wu ZQ, Fang DJ, Jiang DC. 2014. Fast serial analysis of active cholesterol at the plasma membrane in single cells. *Anal. Chem.* 86:678-84
74. Hesari M, Ding ZF. 2016. Review-electrogenerated chemiluminescence: light years ahead. *J. Electro. Soc.* 163:H3116-31
75. Xu JJ, Jiang DP, Qin YL, Xia J, Jiang DC, et al. 2017. C<sub>3</sub>N<sub>4</sub> nanosheet modified microwell array with enhanced electrochemiluminescence for total analysis of cholesterol at single cells. *Anal. Chem.* 89:2216-20
76. Xu JJ, Huang PY, Qin YL, Jiang DC, Chen HY. 2016. Analysis of intracellular glucose at single cells using electrochemiluminescence imaging. *Anal. Chem.* 88:4609-12
77. Zuo HZ, Wang R, Jiang DC, Fang DJ. 2017. Determining the composition of active cholesterol in the plasma membrane of single cells by using electrochemiluminescence. *Chem. Electro. Chem.* 4:1677-8075
78. Xia J, Zhou JY, Zhang RG, Jiang DC, Jiang DP. 2018. Gold-coated polydimethylsiloxane

- microwells for high-throughput electrochemiluminescence analysis of intracellular glucose at single cells. *Anal. Bioanal. Chem.* 410:4787-92
79. Liu G, Ma C, Jin BK, Chen Z, Zhu JJ. 2018. Direct Electrochemiluminescence imaging of a single cell on a chitosan film modified electrode. *Anal. Chem.* 90:4801-6
80. He RQ, Tang HF, Jiang DC, Chen HY. 2016. Electrochemical visualization of intracellular hydrogen peroxide at single cells. 88:2006-9
81. Valenti G, Scarabino S, Goudeau B, Lesch A, Jović M, et al. 2017. Single cell electrochemiluminescence imaging: from the proof-of-concept to disposable device-based analysis. *J. Am. Chem. Soc.* 139:16830-7
82. Cao JT, Wang YL, Zhang JJ, Dong YX, Liu FR, et al. 2018. Immuno-electrochemiluminescent imaging of single cell based on functional nanoprobe of heterogeneous Ru(bpy)<sub>3</sub><sup>2+</sup>@SiO<sub>2</sub>/Au nanoparticles. *Anal. Chem.* 90:10334-9
83. Anderson TJ, Zhang B. 2016. Single-nanoparticle electrochemistry through immobilization and collision. *Acc. Chem. Res.* 49:2625-31
84. Mirkin MV, Sun T, Yu Y, Zhou M. 2016. Electrochemistry at one nanoparticle. *Acc. Chem. Res.* 49:2328-35
85. Chang YL, Palacios RE, Fan FR, Bard AJ, Barbara PF. 2008. Electrogenated chemiluminescence of single conjugated polymer nanoparticles. *J. Am. Chem. Soc.* 130:8906-7
86. Fan FR, Park S, Zhu Y, Ruoff RS, Bard AJ. 2009. Electrogenated chemiluminescence of partially oxidized highly oriented pyrolytic graphite surfaces and of graphene oxide nanoparticles. *J. Am. Chem. Soc.* 131:937-9
87. Dolci LS, Zamarini S, Della Ciana L, Paolucci F, Roda A. 2009. Development of a new device for ultrasensitive electrochemiluminescence microscopy imaging. *Anal. Chem.* 81:6234-41
88. Chen Y, Fu JJ, Cui C, Jiang DC, Chen ZX, et al. 2018. In situ visualization of electrocatalytic reaction activity at quantum dots for water oxidation. *Anal. Chem.* 90:8635-41
89. Pan SL, Liu J, Hill CM. 2015. Observation of local redox events at individual Au nanoparticles using electrogenerated chemiluminescence microscopy. *J. Phys. Chem. C.* 119:27095-103
90. Wilson AJ, Marchuk K, Willets KA. 2015. Imaging electrogenerated chemiluminescence at single gold nanowire electrodes. *Nano Lett.* 15:6110-5
91. Zhu MJ, Pan JB, Wu ZQ, Gao XY, Zhao W, et al. 2018. Electrogenated chemiluminescence imaging of electrocatalysis at a single Au-Pt janus nanoparticle. *Angew. Chem. Int. Ed.* 57:4010-4
92. Ma C, Wu WW, Li LL, Wu SJ, Zhang JR, et al. 2018. Dynamically imaging collision electrochemistry of single electrochemiluminescence nano-emitters. *Chem. Sci.* 9:6167-75

Figure 1. Main ECL mechanistic pathways for  $[\text{Ru}(\text{bpy})_3]^{2+}/\text{TPrA}$  and luminol/ $\text{H}_2\text{O}_2$  systems. (A)  $[\text{Ru}(\text{bpy})_3]^{2+}$  and TPrA are both oxidized at the electrode surface in the “oxidative-reduction” mechanism. (B) ECL emission generated only by TPrA oxidation at the electrode surface and involving the homogeneous reaction of the ruthenium luminophore with the TPrA radicals. Reprinted with permission from ref 8. (C) Luminol anion and hydrogen peroxide are both electrochemically oxidized at the electrode surface emitting the luminescence. (D) Schematic setup used for ECL imaging.

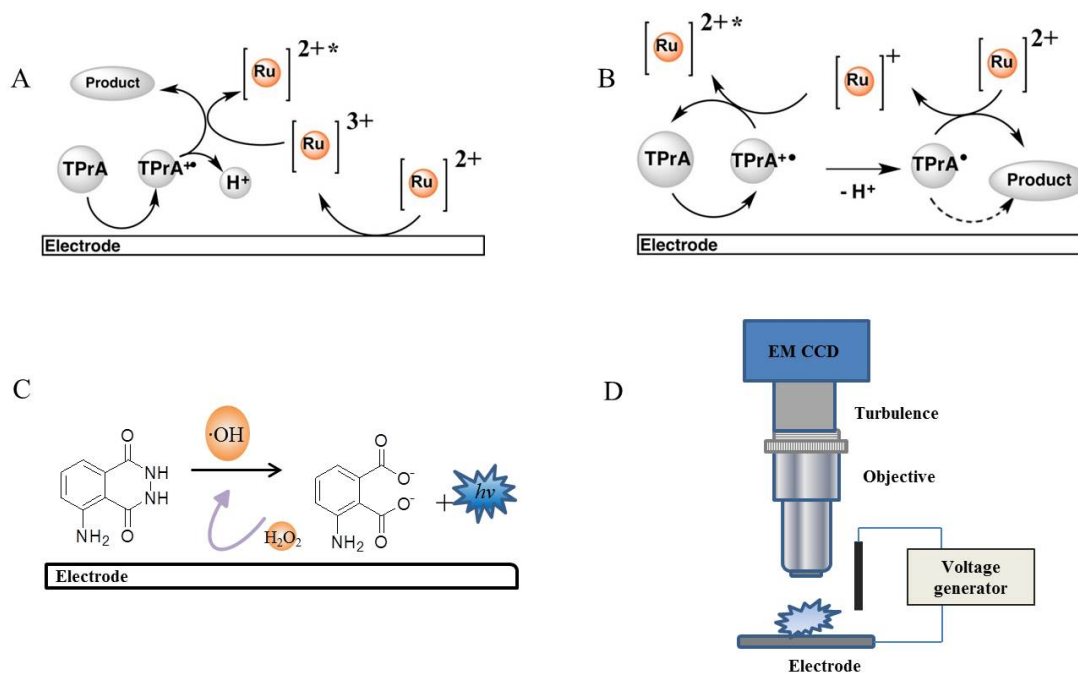


Figure 2. (A) Illustration of the biosensor array with choline oxidase (blue spots), glucose oxidase (green spots) and lactate oxidase (red spots) diagonally immobilized on the working electrodes, and ECL images of choline, glucose and lactate. Reprinted with permission from ref 40. (B) Luminescence image of glucose oxidase-modified nanoneedle electrodes for the response of glucose. Inset: SEM images of nanoneedle electrodes. Reprinted with permission from ref 43. (C) ECL image of the array with 49 individual RuPVP/DNA/enzyme spots containing cyt P450 1B1. Reprinted with permission from ref 46. (D) Representative ECL images of the natural fingerprints treated by the multiple-HRP route for the detection of dermcidin. Reprinted with permission from ref 49.

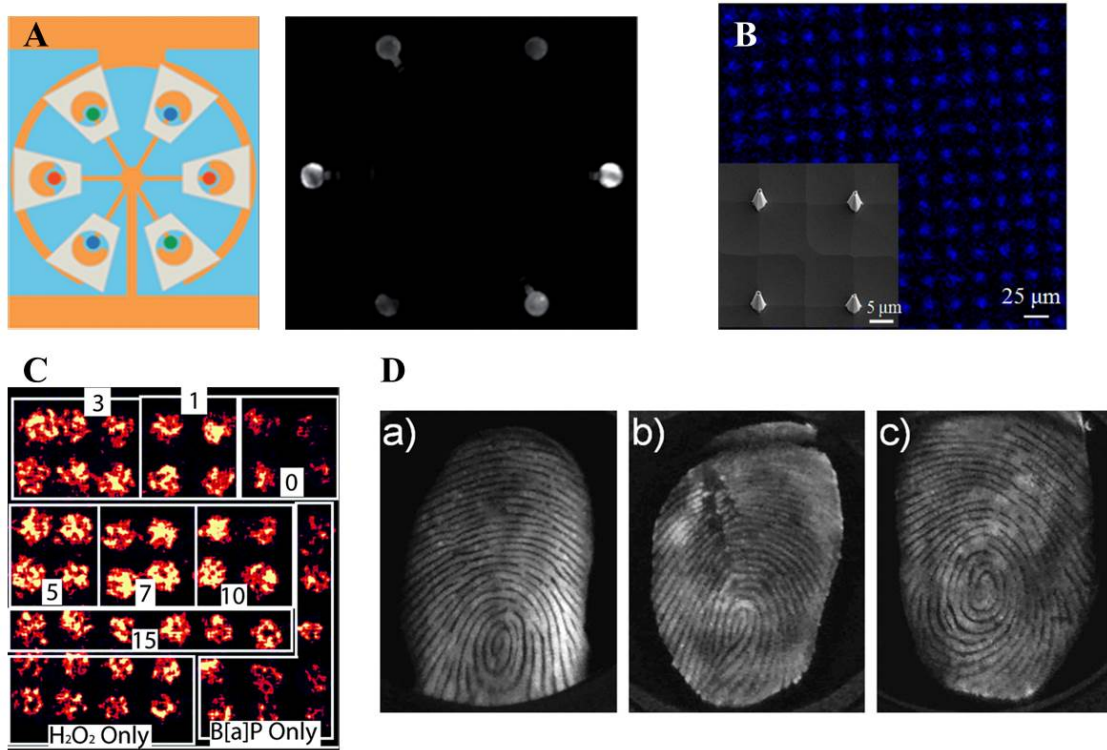


Figure 3. (A) Top-view schematic illustration and ECL imaging of the bipolar electrodes at 22.0 V. Reprinted with permission from ref 55. (B) Micrograph of an interchannel BPE spanning parallel sensing and reporting microchannels (a) and ECL imaging obtained with 0.10 mM (b) and 5.0 mM (c). Reprinted with permission from ref 58. (C) Schematic illustration of the electrical switch fabricated by sandwich immune complex in the channels. Reprinted with permission from ref 61. (D) ECL images on BPE array with increased concentrations of PSA, miRNA-141 and sarcosine. Reprinted with permission from ref 66.

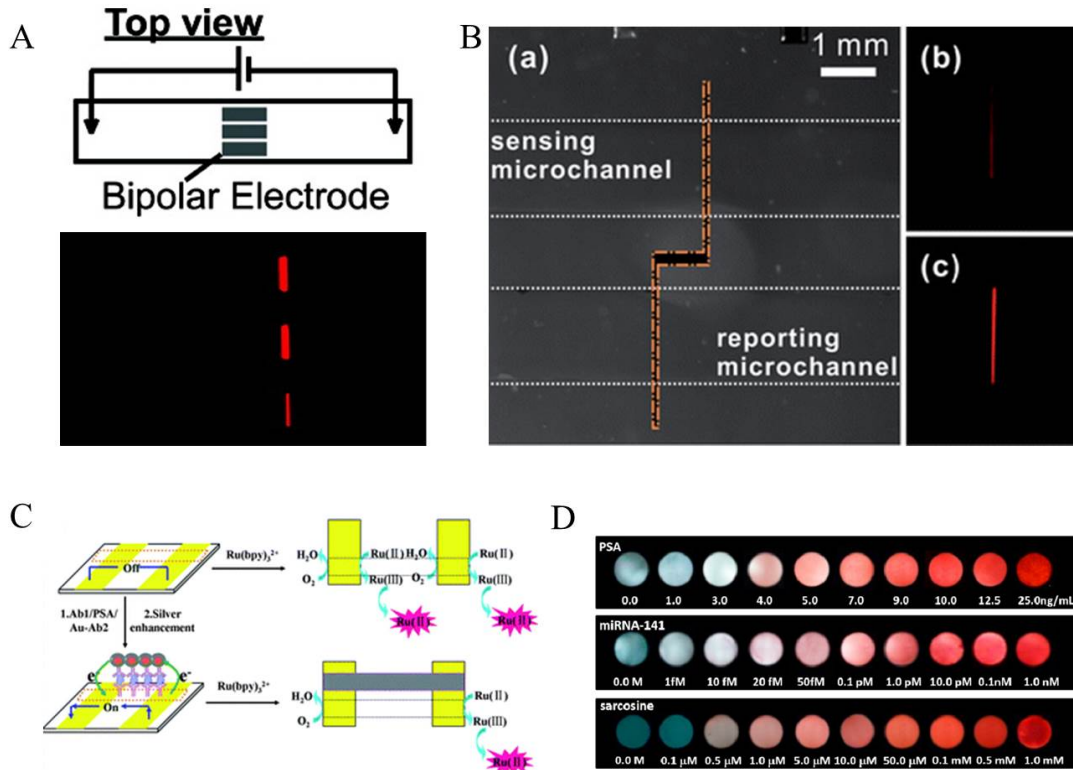


Figure 4.(A) Illustration of ECL imaging for parallel measurement at single cells using luminol/hydrogen peroxide system; (B) ECL imaging of intracellular glucose at single cells retained in the microwells. Reprinted with permission from ref 75; (C) ECL imaging of the efflux of hydrogen peroxide from single cells. Reprinted with permission from ref 34. (D) ECL imaging of intracellular hydrogen peroxide using luminol modified microelectrodes . Reprinted with permission from ref 80. (E) PL (a), ECL (b) and the overlaying (c) images of CHO cells grown on a GC electrode. Reprinted with permission from ref 81.

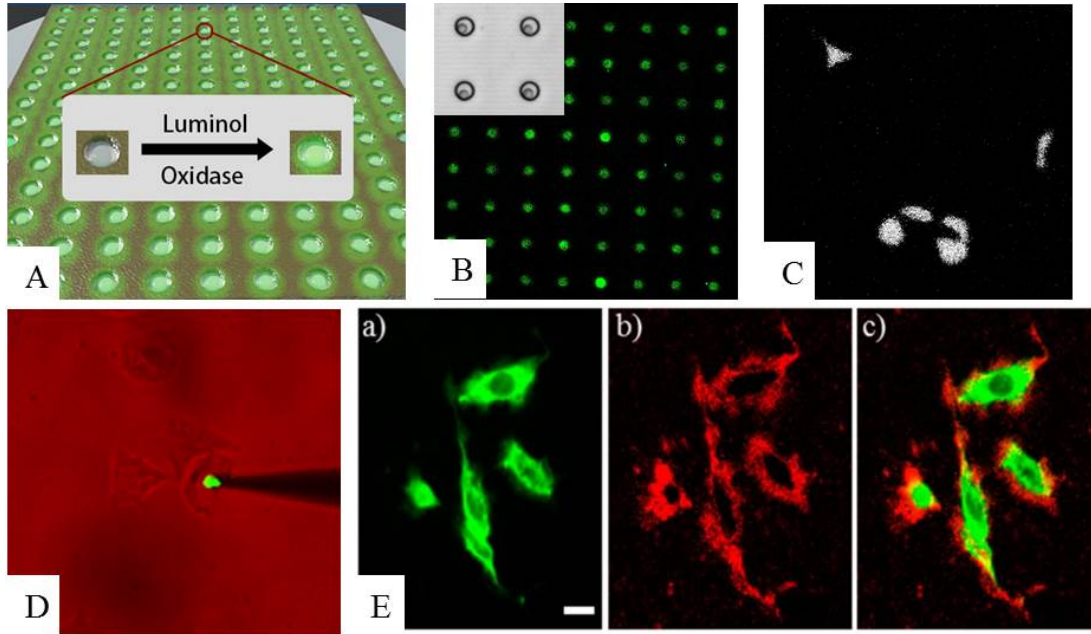


Figure 5. (A) ECL imaging of multiplexed sandwich immunoassays to a sample solution containing IL-8, TIMP-1 and VEGF. Reprinted with permission from ref 27; (B) ECL images of single QDs loaded particle in L-012 solution with different applied potentials. Reprinted with permission from ref 88; (C) A full ECL image ( $50 \times 50 \mu\text{m}^2$ ) collected from Au NPs with an average particle size of 29 nm deposited onto an ITO electrode. Reprinted with permission from ref 89; (D) ECL snapshots of three RuDSNs colliding with the electrode simultaneously. Reprinted with permission from ref 92.

